Engineering Geology 371 (2026) 108887

Contents lists available at ScienceDirect

Engineering Geology

journal homepage: www.elsevier.com/locate/enggeo

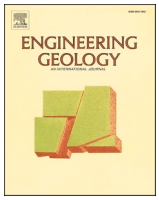

Influence of topsoil depth and rock block content on the stability of soil–rock mixture slopes

Van-Hoa Cao [a], Gyu-Hyun Go [b,*], Sinhang Kang [c]

[a] Institute of Techniques for Special Engineering, Le Quy Don Technical University, Ha Noi 100000, Viet Nam
[b] School of Architecture, Civil and Environmental Engineering, Kumoh National Institute of Technology, Gumi, Gyeongbuk 39177, Republic of Korea
[c] Civil Environmental Engineering, Hannam University, Daejeon 34430, Republic of Korea

ARTICLE INFO

Keywords:
Finite element method
Topsoil depth
Soil–rock mixture slope
Rock block content
Soil–rock interface strength

ABSTRACT

The stability of soil–rock mixture (SRM) slopes is strongly influenced by the heterogeneity of their internal composition and surface geological conditions. This study aims to quantify the effects of topsoil depth, rock block content, and soil–rock interface strength on SRM slope stability. Finite element analyses were conducted using ABAQUS, employing an adaptive automatic stabilization scheme and energy-based failure criteria to evaluate the factor of safety (*FOS*). Scenarios were analyzed by varying topsoil depths and rock block contents of 10%, 20%, 30%, and 40% within the SRM layer. The results indicate that slope stability is weakly influenced by topsoil depth at low rock block contents, but becomes increasingly sensitive as the rock block content increases. For slopes with higher rock block contents, stability decreases even at relatively shallow topsoil depths. However, when the topsoil layer is sufficiently thick, the influence of the rock block content on the *FOS* becomes insignificant. Furthermore, as the contact strength between rock blocks and soil decreases, slope stability also decreases, and this trend decreases with increasing topsoil depths. The novelty of this study lies in explicitly incorporating a surficial residual soil layer within SRM slopes and quantifying its influence on stability. The results provide new insights into slope behavior in weathered residual SRM slopes and support more reliable engineering geological assessments.

1. Introduction

Soil–rock mixture (SRM) slopes are common in both natural and artificial terrains and are widely distributed in mountainous regions (Sun et al., 2014; Cai et al., 2020; Gao et al., 2022). Characterized by heterogeneity and discontinuity, SRMs consist of soils interspersed with solitary rock blocks of varying sizes (Medley and Sanz, 2004; Xu, 2008). The random distribution of soil and rock blocks within the slope makes their mechanical behavior complex, posing significant challenges for slope stability analysis (Wang et al., 2022; Zhao et al., 2023). The failure of SRM slopes can cause severe damage to infrastructure and endanger human lives (Gong et al., 2022; Yang et al., 2022). Therefore, understanding the mechanical properties of SRM slopes is of critical importance.

With the rapid advancement of computational technology and numerical methods, numerical analysis has become a widely used tool for studying slope stability and failure mechanisms in SRMs. Many studies have demonstrated that the presence of solitary rock blocks with certain contents can enhance slope stability while also making potential sliding surfaces more complex and tortuous (Liu et al., 2020; Napoli et al., 2018, 2021; Yang et al., 2021a, 2021b; Zhang et al., 2021a, 2021b; Yu et al., 2023; Cao and Go, 2024, 2025). In addition, rock block morphology and size distribution significantly influence the mechanical behavior and overall stability of SRMs (Lu et al., 2018; Liu et al., 2020; Cao and Go, 2024). The spatial distribution of rock blocks has also been studied through statistical analyses of *FOS* dispersion (Cao and Go, 2025). Findings suggest that when rock block content is low, unfavorable spatial distributions can adversely affect SRM slope stability. Overall, these studies highlight the importance of internal structure in governing both the failure mechanism and stability of SRM slopes, underscoring the importance of selecting modeling methods that accurately reflect the mechanical nature of SRM slopes. Existing modeling methods for simulating SRM internal structure include image-based techniques to reproduce actual rock block morphology (Yang et al., 2021a, 2021b; Zhang et al., 2021a, 2021b), as well as random generation methods that account for variations in block shape, size, and spatial distribution (Yu

* Corresponding author.
E-mail addresses: caovanhoa@lqdtu.edu.vn (V.-H. Cao), gyuhyungo@kumoh.ac.kr (G.-H. Go), sinhang@hnu.kr (S. Kang).

https://doi.org/10.1016/j.enggeo.2026.108887
Received 6 January 2026; Received in revised form 13 April 2026; Accepted 9 June 2026
Available online 11 June 2026

et al., 2023; Wang et al., 2024; Cao and Go, 2024, 2025). Previous studies have primarily focused on investigating the effects of rock block content, size, and shape on the stability of SRM slopes. These studies have demonstrated that the presence of rock blocks within slopes has a significant influence on the mechanical behavior and overall stability of SRM slopes. However, one geological factor frequently encountered in practice but rarely addressed in prior studies is the presence of a topsoil layer covering the SRM.

The formation of a topsoil layer is often associated with long-term biological activity, such as vegetation growth, and natural geological processes. The genesis of SRM also determines its morphological and structural characteristics, which in turn affect its physical and mechanical properties, deformability, and failure mechanisms (Xu and Hu, 2009). SRMs can be classified into several types according to their mode of formation, including gravity accumulation, flow accumulation, glacial deposits, weathered residuals, geological structures, and artificial fills (Zhou et al., 2017). Residual soils are widely distributed and commonly occur in regions prone to slope failures, especially in tropical areas where intense bedrock weathering forms thick residual profiles. Over time, physical, chemical, and biological weathering break down the parent rock while the material remains essentially in place. Depending on the depth and degree of weathering, the materials can be divided into three main categories: residual soil (soil), soil–rock mixture (SRM), and rock mass, as illustrated in Fig. 1 (Brand, 1985; Zhou et al., 2017). The presence of residual soils at the ground surface is often associated with geotechnical engineering problems, particularly those related to soil strength and bearing capacity. Numerous studies have shown that many slope failures and landslide events are closely linked to residual soil layers developed on hillsides. Such mass movements involve the downslope displacement of soil or rock materials when slope stability is compromised due to the disturbance of soil, rock, or weathered constituents (Wibawa et al., 2018).

Many methods have been developed in the past decades to analyze the stability of SRM slopes. The limit equilibrium method (LEM) is widely utilized to evaluate the *FOS* of slopes. The *FOS* value can be determined based on the limit equilibrium, force equilibrium, and moment equilibrium (Abramson et al., 2002; Alok et al., 2024). Although LEM is relatively simple and computationally efficient, applying the prior assumptions to the highly complex and heterogeneous materials of SRM slopes poses a challenge. An effective approach for analyzing the stability of SRM slopes is the finite element method (FEM). In such analyses, the SRM slope model is commonly constructed using digital image processing (DIP) based on field investigation data, or through a random generation method (Gao et al., 2022; Napoli et al., 2018, Napoli et al., 2021; Liu et al., 2018; Yang et al., 2021a, 2021b; Yang et al., 2019). With SRM slope models, rock blocks have randomly distributed shapes and sizes, which can increase the meshing burden. However, this can be overcome and improved (Boulbes, 2020). Another approach involves constructing an SRM slope model using a two-phase random field (Liu et al., 2018; He et al., 2024). The FDM has also been effectively used to analyze the stability of SRM slopes (Zhang et al., 2021a, 2021b; Liu et al., 2020). In addition, the discrete element method (DEM) also provides a promising tool for analyzing the stability of SRM slopes (Gao et al., 2022; Yu et al., 2023; Lu et al., 2018; Hu and Lu, 2023). However, it is not easy to simulate SRM slope models at an engineering scale with reasonable computational resources. During the modeling process, the soil particle size is often increased to reduce the total number of particles in the DEM model, which can alter the soil-rock mixture structure and lead to discrepancies between the numerical model and reality (Li et al., 2024). Overall, each numerical method presents its own advantages and limitations; within the scope of this study, the FEM implemented in ABAQUS is adopted. ABAQUS software offers significant advantages over conventional FEM software, especially in the field of geotechnical engineering. Its superior ability to handle complex, nonlinear behaviors typical of soil and rock materials makes it popular in simulating a wide range of geotechnical problems (Augarde et al., 2021; Xu and Dai, 2017; Dyson and Tolooiyan, 2018, 2019; Liu et al., 2020; Gao et al., 2021; Yang et al., 2021b). Besides, ABAQUS supports powerful integration with Python, allowing automation of modeling and analysis processes. This integration significantly improves work efficiency, especially when dealing with multiple or extremely complex models. Furthermore, user subroutines allow users to customize and extend the built-in functionality of the software by incorporating their algorithms, material models, or boundary conditions. These programs provide the flexibility to solve specific research or engineering problems beyond the standard capabilities of ABAQUS.

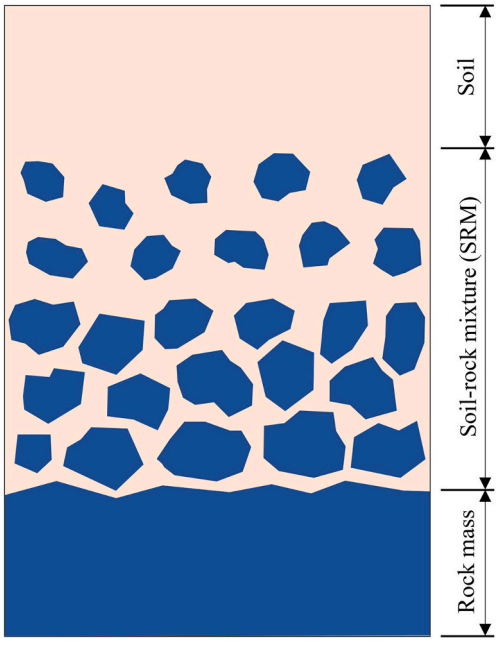

Fig. 1. Soil–rock mixtures formed by weathered residual soils (Zhou et al., 2017).

Previous studies have provided valuable insights into the stability of SRM slopes; however, analyses of weathered residual SRM slopes have rarely accounted for the combined effects of structural heterogeneity and the presence of a surficial residual soil layer (topsoil layer). This study addresses this gap by incorporating a surface residual soil layer with varying thickness (topsoil depth) into the slope model. To achieve this, a Python script was built within ABAQUS to generate geologically consistent slope models, allowing systematic variation of rock block content, topsoil depth, and soil–rock interface strength. Finite element analyses using ABAQUS were then conducted to quantify their combined influence on slope stability.

2. Description of SRM model generation

2.1. Rock shape generation and size distribution

Convex polygonal rock blocks can be generated using a specified set of vertices, as demonstrated by Xu et al. (2016). An alternative method employs random radii and angles in polar coordinates, which provides greater flexibility in adjusting block shapes and allows the creation of non-convex polygons. This approach may more accurately represent the actual shapes of rock blocks (Wang et al., 1999; Meng et al., 2018; Huang et al., 2021; Yu et al., 2023; Cao and Go, 2024). The procedure for generating random rock block shapes in the slope domain involved the following steps:

(1) Step 1: A set of random polar angles was generated for each rock block, following the method proposed by Wang et al. (1999). The random angle for the i-th vertex, $\Delta\theta_i$, is defined as the difference

between the polar angles of two consecutive vertices ($\Delta\theta_i = \theta_{i+1}$ - θ_i):

$$\Delta\theta_i = \frac{2\pi}{n} + (2\zeta - 1).\delta.\frac{2\pi}{n} \quad (1)$$

where δ is the amplification coefficient for the random angle, ranging from 0 to 1, ζ is a random number between 0 and 1, and n is the total number of angles. A lower δ produces more uniform angles. To ensure polygon closure, the angles were adjusted as follows:

$$\Delta\bar{\theta}_i = \frac{2\pi.\Delta\theta_i}{\sum_{j=1}^{n}\Delta\theta_j} \quad (2)$$

The adjusted polar angles θ_i for the polygonal rock block were then determined as follows:

$$\theta_i = \sum_{j=1}^{i-1}\Delta\bar{\theta}_j \quad (3)$$

(2) Step 2: The coordinates of the block vertices were calculated in a Cartesian x–y coordinate system. The vertices were positioned on an ellipse centered at $O(0,0)$, with semi-major axis a and semi-minor axis b ($a \geq b$). To create blocks with concave–convex surfaces, the vertices were distributed across ellipses with varying parameters, as illustrated in Fig. 2. The semi-major axis ranged from $a - \Delta a$ to a, and the semi-minor axis from $b - \Delta b$ to b. These values were determined as follows:

$$\begin{cases} x_i = [a - random(0, \Delta a)]\cos\theta_i \\ y_i = [b - random(0, \Delta b)]\cos\theta_i \end{cases} \quad (4)$$

The rock blocks were assigned random orientations by rotating them about their centers, with coordinates determined as follows:

$$\begin{cases} x'_i = x_i\cos\alpha_i - y_i\sin\alpha_i \\ y'_i = x_i\sin\alpha_i - y_i\cos\alpha_i \end{cases} \quad (5)$$

where α_i is a phase angle determining the orientation of the i-th rock block, ranging from 0 to 2π. The area of the polygon can then be determined as follows:

$$A_i = \frac{1}{2}\sum_{I=1}^{n}(x_i y_{i+1} - x_{i+1}y_i) \quad (6)$$

The number of edges for each block (n) was based on the assumption that larger blocks typically have more edges, while smaller blocks have fewer (Cheng et al., 2023). In this study, blocks were generated with six to eighteen edges.

The rock block size distribution ranged from 0.05Lc to 0.75Lc, where Lc is the height of the SRM slope (Napoli et al., 2018; Zhao et al., 2022). Given the SRM slope height of 10 m, block sizes ranged between 0.5 m and 7.5 m. In this study, block size was characterized by the major axis length of the ellipse used to generate each block. The aspect ratio of a block was defined as $k = a/b$ (Wang et al., 2014; Liu et al., 2020).

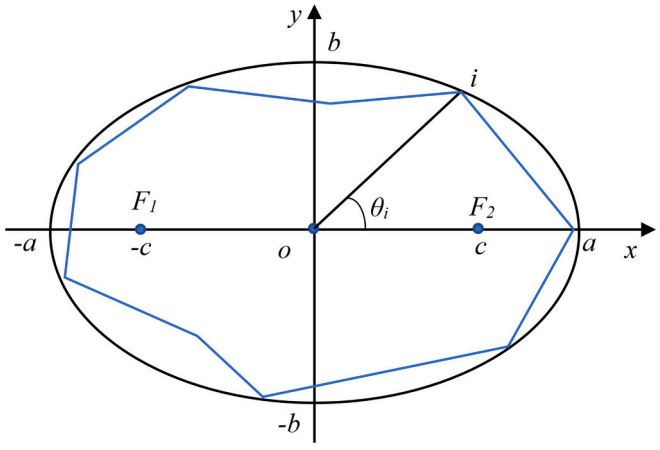

Fig. 2. Vertex coordinates of the polygon defining the non-convex blocks generated by random variables. The ellipse foci are (±c, 0), where c = $(a^2\text{-}b^2)^{0.5}$.

2.2. Position definition of rock blocks and overlap checking

Due to the inherent randomness of rock block distribution in SRM slopes, block centers were randomly and uniformly distributed across the model domain. To check for overlaps between two blocks (i and j), the intersection of rock block i with the ellipse defining rock block j (and vice versa) was examined (Fig. 3). Vertex M lies outside a rock block if the following condition is satisfied:

$$F_1M + F_2M > 2a \quad (7)$$

where F_1 and F_2 represent the foci of the ellipse, as described in Section 2.1. After the rock block is rotated and translated, the corresponding focal coordinates are given by F_1 ($x - c.cos\alpha$, $y - c.sin\alpha$) và F_2 ($x + c.cos\alpha$, $y + c.sin\alpha$) where $c = (a^2 - b^2)^{1/2}$. Once the coordinates of F_1, F_2, and point M are determined, Eq. 7 is implemented in the Python script.

According to Brand (1985), weathering profiles in Hong Kong typically comprise a near-surface SRM layer with a rock block content of less than 50%, in which the rock blocks are predominantly isolated and unbonded. This is underlain by an SRM layer with a higher rock block content (>50%), where interlocking between blocks becomes more significant. The study also indicates that most slope failures in the region are shallow, with failure depths generally not exceeding 3.0 m. A similar study by Zhou et al. (2017) reported comparable geological characteristics, characterized by low rock block content and loosely distributed blocks near the ground surface, indicating that slope stability is primarily governed by the near-surface layer. Therefore, in the present study, the thickness of the topsoil layer is limited to a maximum of 3.0 m, while the SRM is considered with a rock block content of up to 40%, without accounting for interlocking between rock blocks. To ensure a sufficient gap between rock blocks during the preprocessing stage, thereby reducing the computational burden associated with mesh generation, a special treatment technique based on the study of Wang et al. (1999) was adopted. Specifically, a scaling factor was applied to enlarge the rock block sizes while preserving their original shapes before overlap checking. In this study, the scaling factor was set to 1.1.

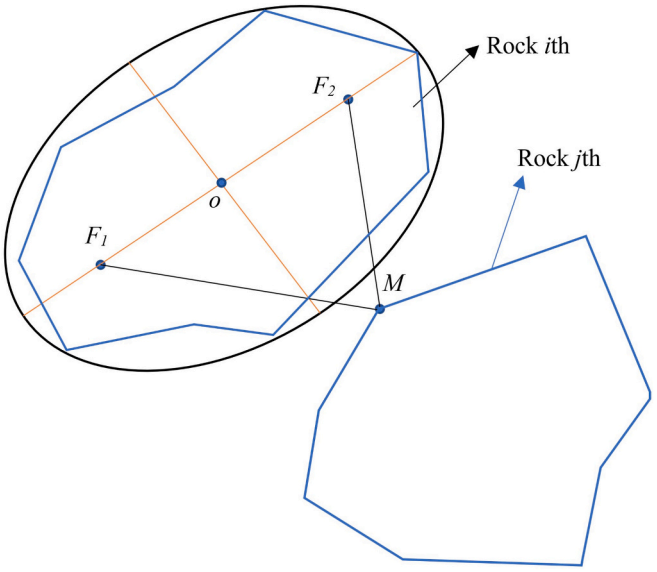

Fig. 3. Positioning of rock blocks and overlap verification between adjacent blocks.

2.3. Establishment of SRM slope

The SRM slope model is automatically generated through a Python script implemented in ABAQUS, which enables the systematic and reproducible generation of slope models incorporating varying topsoil depths and random rock block distributions. Fig. 4 presents the overall procedure for generating the SRM slope model, and the detailed modeling steps are outlined below.

1- Determine the input parameters of the model, including the content, shape, and size of rock blocks, the number of rock block groups, and the thickness of the topsoil layer.
2- Generate the i-th rock block group, in which block sizes are distributed within the range d_i to d_{i+1}, with a prescribed total area A_i.
3- Generate rock blocks for group i-th based on the shape parameters defined in Eqs. 1–3. Each rock block is represented as a polygon in a Cartesian coordinate system, with the coordinates of its vertices determined according to Eqs. 4–5.
4- Randomly place the rock blocks within the slope domain based on their centroid coordinates.
5- Check for overlap among rock blocks using the criterion specified in Eq. 7. If overlap occurs, return to Step 3; otherwise, proceed to the next step.
6- Compute the area of the j-th rock block according to Eq. 6 and update the cumulative area of all rock blocks generated in group i.
7- Compare the cumulative rock block area with the prescribed target area A_i. If the requirement is satisfied, return to Step 2 to generate the next rock block group; otherwise, go back to Step 3.
8- Verify whether the required number of rock block groups has been generated. If the condition is not satisfied, repeat the procedure from Step 2; otherwise, terminate the modeling process.

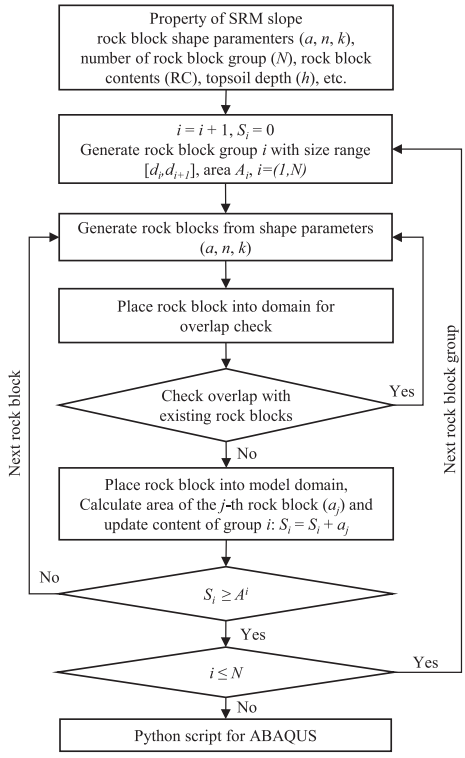

Fig. 4. Flowchart for generating SRM slope models.

3. Slope stability analysis

3.1. Model domain and material properties

A two-dimensional finite element model was developed, consisting of a topsoil layer overlying an SRM layer, with bedrock at the base (Fig. 5). The slope height was 10 m with an inclination of 45°. The topsoil was modeled with uniform thicknesses of 0.1, 0.5, 1.0, 1.5, 2.0, 2.5, and 3.0 m. As the topsoil thickness increased, the SRM layer thickness decreased accordingly. The material properties used in this study are listed in Table 1 (Zhang et al., 2021a, 2021b; Li et al., 2022).

In this work, the SRM layer thickness decreased with increasing h, based on the block size range defined in Section 2.1. The assumed rock block size distribution is illustrated in Fig. 6. The corresponding block shape parameters were $\Delta a/a = 0.25$, $\Delta b/b = 0.25$, and $a/b = [1,2]$. To evaluate the influence of block content on slope stability, four block content levels (10%, 20%, 30%, and 40%) were considered in the SRM layer. Fig. 7 shows examples of slope models with different topsoil depths for a case where the SRM layer contained 30% rock blocks. The interaction between rock blocks and surrounding soil or bedrock was modeled using the contact strength at the soil–rock block interface. This interaction is commonly characterized by the soil–rock interface strength, which may be comparable to the soil strength under tight contact (full contact) conditions or reduced (frictional contact) when the contact is loose. Generally, the friction coefficient at the soil–rock interface varies between 0 and $\tan\phi$, where ϕ denotes the internal friction angle of the surrounding soil (Riedmüller et al., 2001; Khorasani et al., 2019; Wang et al., 2024). In addition, under practical conditions, the soil–rock interface strength may be influenced by moisture conditions and can vary depending on the surface characteristics of the rock blocks; this aspect represents an interesting topic that will be further investigated in our future work. In addition, the geometric characteristics of rock blocks, such as block irregularity, can enhance interlocking and shear strength of SRM, thereby contributing to improved slope stability (Cao and Go, 2024). In this study, the random shapes of rock blocks are represented through shape parameters that have been defined and presented in the preceding sections.

3.2. Finite element method for slope stability

FEM is extensively used in geotechnical engineering (Augarde et al., 2021). In this study, analyses were performed in ABAQUS, which supports automated modeling using Python scripting and user-defined subroutines. To minimize local instability and computational cost, Abaqus/Standard offers an automatic mechanism for reducing the instabilities of quasi-static problems by automatically setting volume-proportional damping to the model without notably affecting the solution. The parameter c is chosen so that the dissipated energy in a given increment with characteristics similar to the first increment is a tiny proportion of the extrapolated strain energy. This dissipated energy fraction is set to 2.0×10^{-4} as a default applied in the present work. With the adaptive automatic stabilization scheme, parameter c is changed according to spatial and time. This process is controlled by the ratio of the static dissipation energy (ALLSD) to total strain energy (ALLIE) and the convergence history. The (ALLSD/ALLIE) ratio is

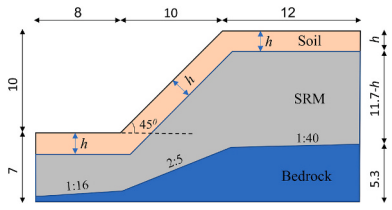

Fig. 5. Geometric dimensions of the simulation model.

Table 1
Material properties used in the slope stability analyses.

Material	Density (kg/m^3)	Young's modulus (MPa)	Poisson's ratio	Internal friction angle (°)	Cohesion (kPa)
Soil	2000	200	0.3	20	15
Rock	2400	20,000	0.2	42	900

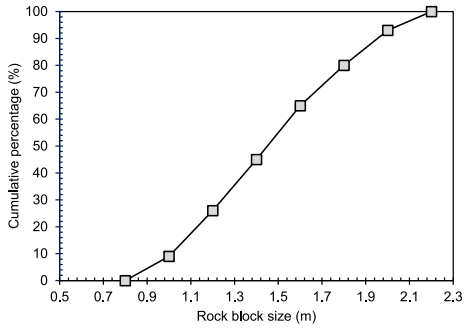

Fig. 6. Size distribution of rock blocks.

restrained by a predefined accuracy tolerance. If this ratio for the whole model overs the accuracy tolerance, c at each element will be adjusted to ensure that it is lower than the tolerance at both the local and global element levels. This ratio should be as low as feasible to achieve accuracy. The accuracy tolerance in the adaptive automated stabilization system is set to 5% by default, which is appropriate for the majority of complex scenarios (Abaqus, 2018; Boulbes, 2020). To improve the accuracy of the analytical data, the accuracy tolerance value was adjusted to 2% in the current investigation. The static equilibrium equation incorporating an artificial damping coefficient can be expressed as follows:

$$P - I - c.M^{*}.\frac{\Delta u}{\Delta t} = 0 \tag{8}$$

where $\Delta u/\Delta t$ is the vector of nodal velocities, Δu is the nodal displacement increment, Δt is the time increment, P is the external force, I is the internal nodal force, c is an artificial damping factor, and M^* is an artificial mass matrix derived from unit density. The artificial viscous force, expressed as $c.M^*.(\Delta u/\Delta t)$, provides numerical stability during the solution process.

3.3. Strength reduction method and slope failure criterion

In finite element–based slope stability analyses, the *FOS* is typically evaluated by coupling the strength reduction method with a specified failure criterion. The shear strength reduction method is widely applied in slope stability analyses using finite element modeling (Griffiths and Lane, 1999; Zheng et al., 2005; Yang et al., 2019; Sun et al., 2020). This technique is based on incrementally decreasing the shear strength of slope materials until failure occurs, using a strength reduction factor (SRF). The reduction process is expressed as follows:

$$c_i = \frac{c}{SRF_i}, \phi_i = \arctan\left(\frac{\tan\phi}{SRF_i}\right) \tag{9}$$

where c and ϕ represent the actual or initial values of soil cohesion and internal friction angle, respectively, and c_i and ϕ_i denote the reduced shear strength parameters corresponding to SRF_i. The SRF_i value at which slope failure occurs is defined as the factor of safety of the slope.

When applied to materials following the Mohr–Coulomb failure criterion, shear strength of the material gradually decreases with increasing *SRF*, whereas Poisson's ratio (ν) remains constant. This can lead to the formation of a spurious plastic zone deep within the slope, potentially resulting in inaccurate *FOS* values. Zheng et al. (2005) proposed mitigating this issue by reducing Poisson's ratio during the strength-reduction procedure, ensuring compliance with the following inequality:

$$\sin\phi \geq 1\text{-}2\nu \tag{10}$$

To identify slope failure, several criteria have been proposed, including (1) non-convergence of the numerical solution (Zienkiewicz et al., 1975; Dawson et al., 1999), (2) development of plastic deformation zones within the slope (Zheng et al., 2005), (3) rapid increases in the displacement of monitoring points (Zhang and Zhang, 2022), and (4) changes in model energy components (Tu et al., 2016; Huang et al., 2020; Hua et al., 2022; Zou et al., 2023).

Although several criteria have been widely used to define slope

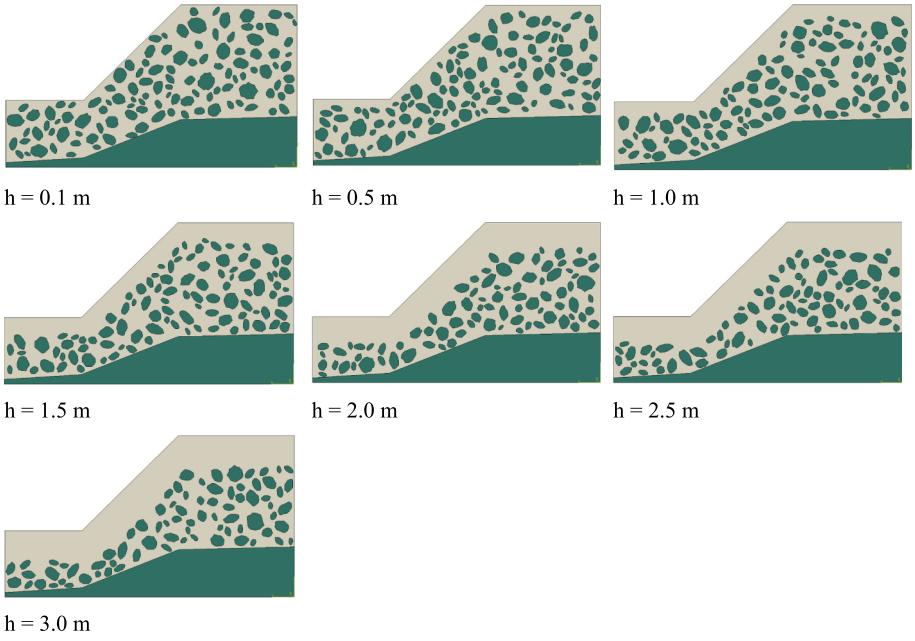

Fig. 7. SRM slope models with seven different topsoil depths (0.1, 0.5, 1.0, 1.5, 2.0, 2.5, and 3.0 m) and a constant rock block content of 30%.

failure, each has inherent limitations that hinder a consistent and objective determination of the FOS. The non-convergence criterion lacks clear physical meaning, as non-convergence may arise from multiple factors and does not necessarily indicate actual collapse, potentially leading to an underestimation of the *FOS*. The plastic zone criterion is difficult to quantify, while the displacement-based criterion depends strongly on the selection of monitoring points (Huang et al., 2020; Hua et al., 2022; Zou et al., 2023). To address these limitations, an energy-based criterion is adopted, in which the *FOS* is defined as the strength reduction factor (*SRF*) at which the plastic dissipation energy first equals or exceeds the elastic strain energy (ALLPD ≥ ALLSE). This approach has been validated for both homogeneous soil slopes and SRM slopes (Cao and Go, 2025). The strength reduction technique and FOS determination are automated through a coupled subroutine (USDFLD and URDFIL). Specifically, USDFLD is used to update material properties by applying the strength reduction factor at each analysis step, while URDFIL reads the output database (.fil) to monitor the evolution of energy components throughout the analysis. Once the failure criterion is satisfied, URDFIL terminates the analysis and outputs the corresponding FOS, thereby significantly reducing post-processing effort. The overall workflow is summarized in Fig. 8.

3.4. Validation

In this study, stability analyses of an SRM slope were conducted in ABAQUS under two-dimensional plane strain conditions for perfectly elastic–plastic materials subjected to gravity loading. The Mohr–Coulomb failure criterion and unbounded flow rule were adopted, consistent with previous studies (Zheng et al., 2005; Griffiths and Lane, 1999). The Mohr–Coulomb plasticity model, which is widely used to describe the behavior of soil or rock, is available in ABAQUS with the parameters described in Section 3.1. Boundary conditions were applied as fixed constraints at the slope base and rollers along both lateral boundaries. Four-node bilinear plane strain quadrilateral elements (CPE4) were used.

To verify the calculation results using FEM in ABAQUS and the appropriate element mesh size, a mesh convergence study was also conducted for the SRM slope with a topsoil layer depth of 1.0 m and a rock block content of 20%. As the minimum equivalent diameter of rock blocks in the slope domain is 0.8 m, the mesh size was chosen to vary between 0.2 m and 0.7 m. The result indicated that the change in *FOS* is negligible for mesh sizes ranging from 0.2 m to 0.3 m (Fig. 9). Therefore, an approximate global mesh size of 0.2 m can be suitable for SRM slopes in this study. Furthermore, with the automatic meshing feature in ABAQUS, the meshing process is automatically conducted to consider the location, shape, and size of the rock blocks in the slope, ensuring the approximate global mesh size meets the preset value. In addition, to further verify the applicability of the method adopted in the present study, a slope model without the SRM layer was analyzed for validation purposes. The *FOS* is 1.122, which is in close agreement with the value of 1.105 obtained from an equivalent model analyzed using the modified Bishop method (Li et al., 2022), with a deviation of 1.54%. Furthermore, a slope model was also analyzed without considering the artificial damping coefficient. The analysis results are presented in Fig. 10. The computed *FOS* is 1.208, compared with an *FOS* value of 1.230 obtained using the method proposed in this study. The difference between the two results is 1.79%, indicating that the proposed method provides reliable results.

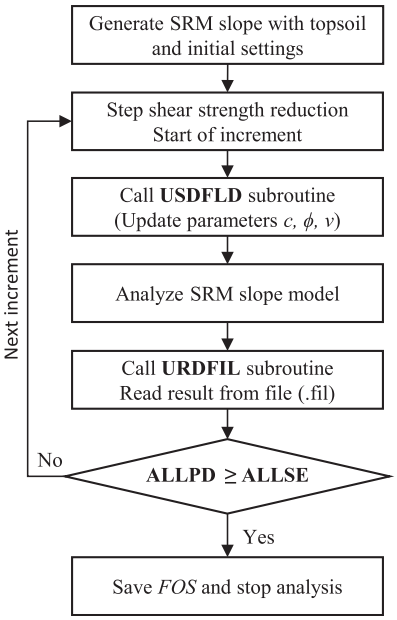

Fig. 8. Flowchart for determining FOS using ABAQUS/Standard.

4. Results and discussion

4.1. Influence of topsoil layer depth

To assess the influence of topsoil thickness on SRM slope stability, 20 analytical models were developed for each topsoil depth (0.1, 0.5, 1.0, 1.5, 2.0, 2.5, and 3.0 m). The models followed the setup described in Section 3.1, with the rock block content in the SRM layer fixed at 30%. The stability analysis results and corresponding *FOS* values are presented in Table 2, and a box plot of the *FOS* distribution across different topsoil depths is shown in Fig. 11. The interquartile range (*IQR*) method was applied to identify outliers significantly deviating from the dataset (Dekking, 2005).

The results indicate that when topsoil depth increases from 0.1 m to 1.5 m, *FOS* values remain nearly constant. This suggests that a shallow topsoil layer has little effect on SRM slope stability. The presence of rock blocks in the central region of the slope helps prevent the propagation of a plastic zone from the toe to the crest, thereby enhancing stability—a finding consistent with previous studies (Peng et al., 2022; Wang et al., 2024). Equivalent plastic strain contours also showed notable similarities for slopes with topsoil depths ≤1.5 m, where the potential sliding surface was more irregular. The first 5 cases for slopes with 0.1 m and 1.5 m of topsoil are illustrated specifically in Figs. 12(a) and (b).

In contrast, when the topsoil thickness exceeded 1.5 m, *FOS* values decreased markedly with further increases in depth. This indicates that the stabilizing effect of the SRM layer diminishes as the overlying topsoil becomes thicker. This behavior can be attributed to an increase in the thickness of the topsoil layer, which causes the SRM layer to be positioned deeper within the slope domain. Consequently, the region of rock blocks providing resistance against the development of the plastic zone is reduced, leading to a decrease in slope stability. In these cases, the potential sliding surface was concentrated primarily within the topsoil, as observed in most models (Figs. 13(a) and (b)), leading to reduced

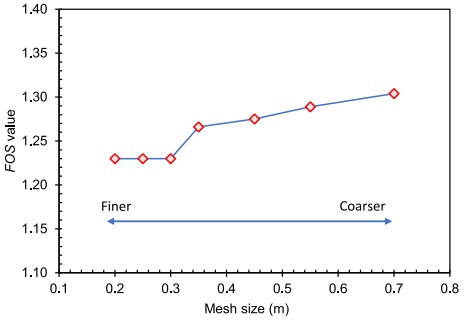

Fig. 9. Mesh convergence study.

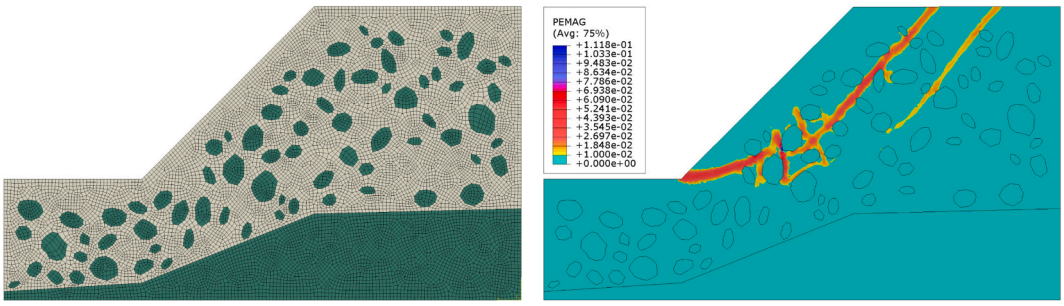

Fig. 10. SRM slope with $h = 1.0$ m: (a) Finite element mesh with an approximate global size of 0.2 m, (b) Equivalent plastic strain contours.

Table 2
FOS for twenty stochastic SRM slope models with seven topsoil depths ($h = 0.1$, 0.5, 1.0, 1.5, 2.0, 2.5, and 3.0 m) and a rock block content of 30%.

No.	*h* (m)						
	0.1	0.5	1.0	1.5	2.0	2.5	3.0
1	1.273	1.203	1.249	1.200	1.261	1.171	1.118
2	1.250	1.312	1.227	1.230	1.164	1.184	1.110
3	1.227	1.220	1.286	1.220	1.179	1.159	1.103
4	1.212	1.312	1.227	1.282	1.254	1.159	1.125
5	1.219	1.273	1.202	1.259	1.238	1.171	1.138
6	1.268	1.232	1.276	1.214	1.189	1.171	1.105
7	1.286	1.278	1.232	1.205	1.203	1.180	1.135
8	1.227	1.302	1.227	1.236	1.197	1.159	1.134
9	1.278	1.211	1.243	1.262	1.234	1.183	1.135
10	1.248	1.266	1.273	1.292	1.192	1.171	1.144
11	1.259	1.238	1.230	1.174	1.223	1.171	1.110
12	1.174	1.170	1.253	1.266	1.168	1.177	1.139
13	1.226	1.215	1.191	1.224	1.231	1.170	1.134
14	1.184	1.227	1.177	1.298	1.180	1.177	1.134
15	1.249	1.302	1.269	1.275	1.206	1.171	1.144
16	1.220	1.224	1.257	1.224	1.190	1.159	1.135
17	1.272	1.268	1.187	1.216	1.177	1.159	1.144
18	1.175	1.266	1.188	1.229	1.200	1.171	1.115
19	1.236	1.281	1.209	1.187	1.224	1.169	1.135
20	1.233	1.249	1.205	1.232	1.239	1.183	1.140
Mean	1.236	1.253	1.230	1.236	1.208	1.171	1.129
Max	1.286	1.312	1.286	1.298	1.261	1.184	1.144
Min	1.175	1.170	1.177	1.174	1.164	1.159	1.103
SD	0.033	0.040	0.033	0.035	0.029	0.008	0.014

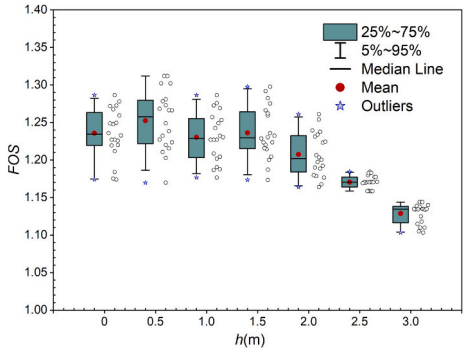

Fig. 11. Box plot of *FOS* values for SRM slopes with seven different topsoil depths ($h = 0.1$, 0.5, 1.0, 1.5, 2.0, 2.5, and 3.0 m) and a constant rock block content of 30%.

overall slope stability. For a topsoil depth of 3.0 m, the sliding surface was located almost entirely within the topsoil layer, forming a smooth, nearly circular slip surface similar to that of a homogeneous soil slope. The mean *FOS* in this case was 1.129, differing by approximately 0.62% from the *FOS* of 1.122 for a slope model without the SRM layer (Section 3.4). Accordingly, the plastic zone, which provides the basis for identifying the potential slip surface of the slope, exhibits a tortuous and complex geometry under shallow topsoil conditions, whereas it tends to evolve into a circular slip surface when the topsoil layer is deep. In practice, the mechanical behavior of the surficial soil layer may be influenced by factors such as vegetation, moisture content, compaction, and cracking, which can either enhance or reduce slope stability, particularly for greater soil thicknesses. These effects can be incorporated into the analysis by appropriately modifying the material properties of the surficial soil layer, thereby improving the applicability of the numerical results to real field conditions.

4.2. Influence of rock content

To further examine the influence of rock block content in the SRM layer, additional analyses were conducted with contents of 10%, 20%, and 40%, while varying topsoil thickness. Statistical indicators of *FOS*, including mean, maximum, minimum, and standard deviation (*SD*), are provided in Tables 3–5. Box plots of the statistical *FOS* values for each case are shown in Figs. 14–16, and Fig. 17 illustrates the relationships between topsoil thickness, mean *FOS*, and *SD* across different block contents. The mean *FOS* and *SD* were calculated using all computed *FOS* values for each case without excluding the identified outliers.

For rock block contents of 10%, 20%, and 30%, slope stability exhibited a consistent trend: *FOS* values remained largely unchanged when the topsoil thickness was $\leq$1.5 m (Figs. 14–17(a)). However, with 40% rock block content, slope stability decreased significantly when the topsoil depth was $\geq$1.0 m. This suggests that higher block content increases the slope's sensitivity to changes in topsoil thickness compared with lower block contents. This phenomenon can be explained as follows. When the rock block content within the slope is low, the rock blocks are randomly and sparsely distributed, causing the boundary between the topsoil layer and the SRM layer, as well as the mechanical contrast between the two layers, to be poorly defined. However, as the rock block content in the SRM layer increases, specifically to 40%, the distinction between the topsoil layer and the SRM layer becomes more pronounced in terms of both mechanical properties and boundary. Consequently, the influence of the topsoil layer on slope stability becomes significant even when the topsoil thickness is small. Furthermore, when the rock block content reaches 40%, the rock blocks more effectively inhibit the development and propagation of plastic zones within the slope domain, leading to a more tortuous potential failure surface. This results in a more pronounced variation in *FOS* with the thickness of the topsoil layer.

Overall, topsoil thickness had a pronounced influence on SRM slope stability, and this influence intensified with increasing block content (Fig. 17(a)). The stabilizing effect of the SRM layer was gradually offset as the topsoil thickened, and by a depth of 3.0 m, mean *FOS* values across different block contents were no longer significantly different. Within the scope of this study, this indicates that when the topsoil layer

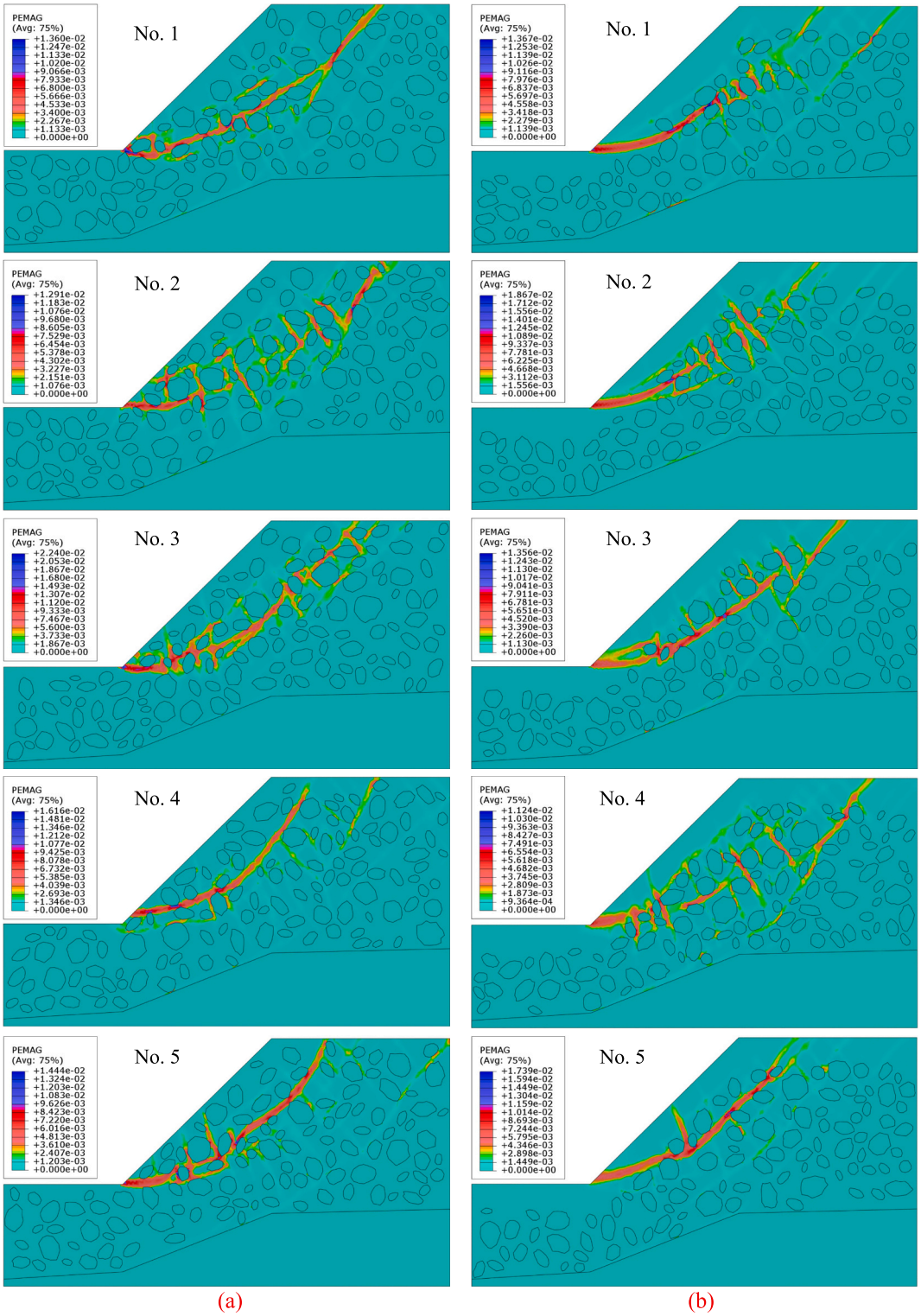

Fig. 12. Equivalent plastic strain contours of the first 5 slope models out of 20 cases with: (a) $h = 0.1$ m, (b) $h = 1.5$ m.

is sufficiently thick (≥3.0 m), the underlying SRM layer exerts minimal influence on overall slope stability, regardless of block content. Furthermore, the dispersion of *FOS* values decreased as topsoil thickness increased (Fig. 17(b)).

4.3. *Influence of soil-rock interfaces*

To investigate the influence of soil–rock block interface conditions on the stability of SRM slopes, Wang et al. (2024) considered different contact conditions, including full contact, frictional contact, and smooth contact. Under full contact, the rock block and surrounding soil remain in tight contact without tangential sliding or separation. In practice,

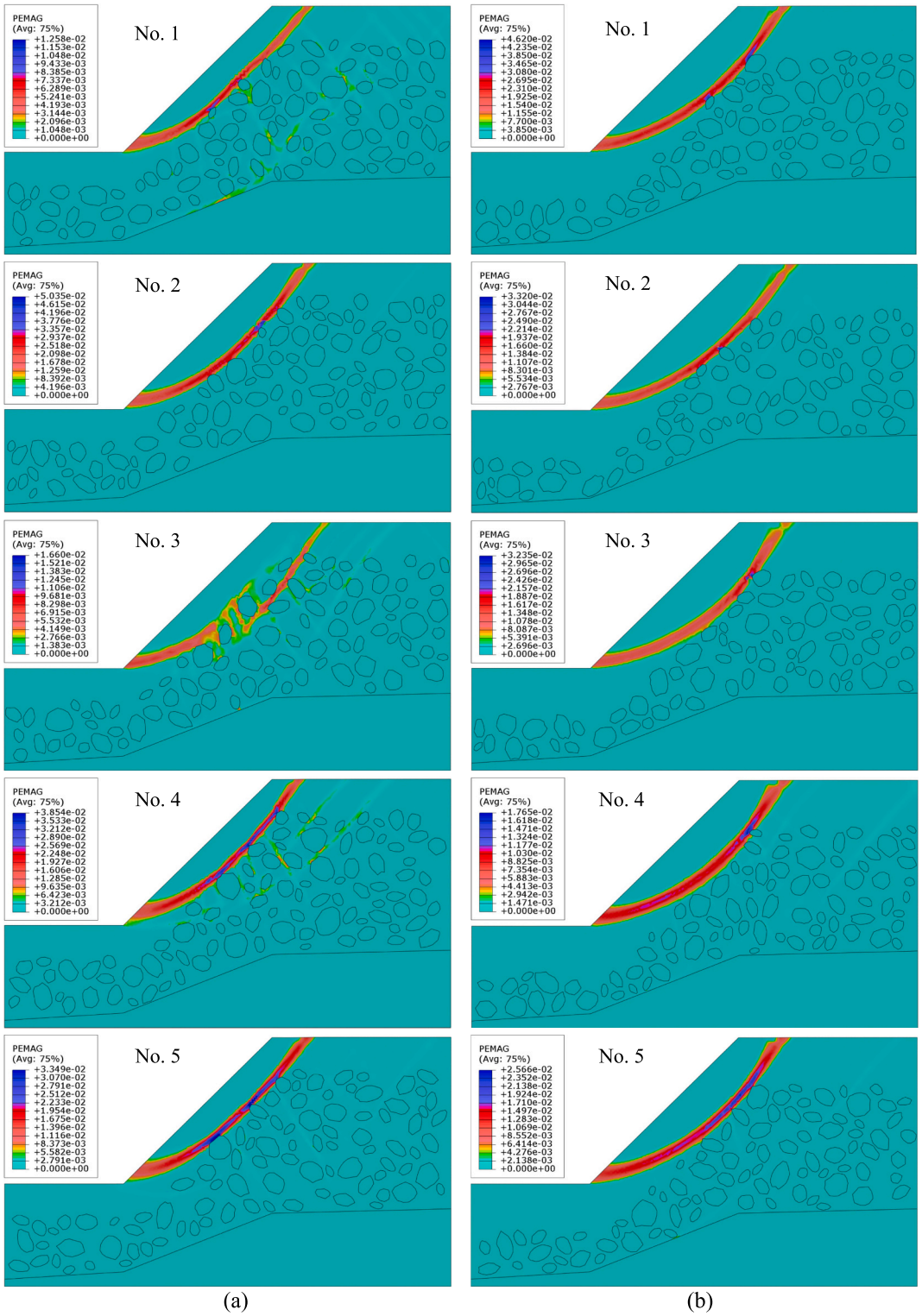

Fig. 13. Equivalent plastic strain contours of the first 5 slope models out of 20 cases with: (a) $h = 2.0$ m, (b) $h = 3.0$ m.

interactions at the soil–rock interface are unavoidable and can be reasonably idealized as frictional contact characterized by a friction coefficient, while a zero friction coefficient represents smooth contact. However, ABAQUS supports automatic assignment of contact conditions only for 3D models. In 2D analyses, contact interactions must be defined manually, which is feasible only for simple geometries. For complex models such as randomly generated SRM slopes, manual assignment becomes impractical, particularly when large numbers of realizations are required for statistical analysis. To address this limitation, the Python script described in Section 2.3 was extended to automatically assign contact interactions between each rock block surface and the surrounding soil, enabling efficient and fully automated model generation.

A sensitivity analysis of soil–rock interface friction was conducted for

Table 3
Statistical measures of *FOS* values obtained for seven different topsoil layer depths (h = 0.1, 0.5, 1.0, 1.5, 2.0, 2.5, and 3.0 m) and a rock block content of 10%.

	h (m)						
	0.1	0.5	1.0	1.5	2.0	2.5	3.0
Mean	1.135	1.130	1.130	1.139	1.133	1.128	1.117
Max	1.199	1.181	1.211	1.199	1.175	1.156	1.133
Min	1.085	1.085	1.081	1.085	1.093	1.094	1.096
SD	0.034	0.028	0.036	0.031	0.023	0.021	0.013

Table 4
Statistical measures of *FOS* values obtained for seven different topsoil layer depths (h = 0.1, 0.5, 1.0, 1.5, 2.0, 2.5, and 3.0 m) and a rock block content of 20%.

	h (m)						
	0.1	0.5	1.0	1.5	2.0	2.5	3.0
Mean	1.178	1.180	1.177	1.174	1.154	1.148	1.120
Max	1.246	1.227	1.250	1.216	1.202	1.177	1.159
Min	1.081	1.105	1.117	1.085	1.102	1.105	1.085
SD	0.037	0.029	0.037	0.035	0.031	0.018	0.018

Table 5
Statistical measures of *FOS* values obtained for seven different topsoil layer depths (h = 0.1, 0.5, 1.0, 1.5, 2.0, 2.5, and 3.0 m) and a rock block content of 40%.

	h (m)						
	0.1	0.5	1.0	1.5	2.0	2.5	3.0
Mean	1.366	1.383	1.388	1.318	1.248	1.173	1.131
Max	1.466	1.464	1.479	1.369	1.291	1.199	1.159
Min	1.305	1.299	1.319	1.189	1.197	1.149	1.105
SD	0.050	0.038	0.045	0.040	0.022	0.016	0.015

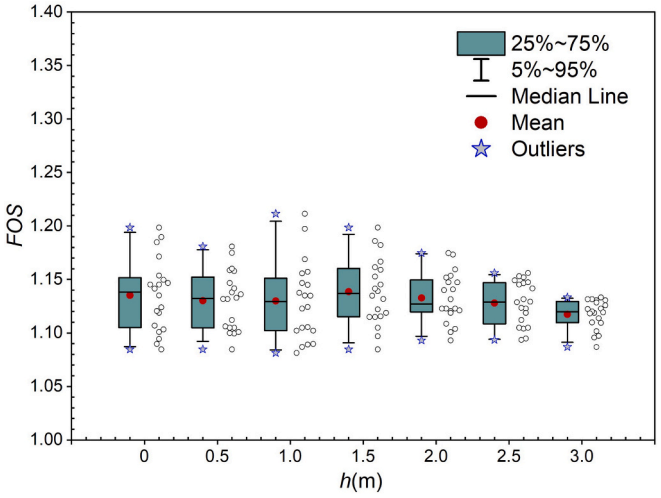

Fig. 14. Box plot of *FOS* values for SRM slopes with seven different topsoil depths (h = 0.1, 0.5, 1.0, 1.5, 2.0, 2.5, and 3.0 m) and a constant rock block content of 10%.

a slope with a topsoil depth of 1.0 m, with the interface friction coefficient varying from $\mu = 0$ (smooth) to 0.25tanϕ', 0.5tanϕ', 0.75tanϕ', and full contact. As illustrated in Fig. 18, the difference between the smooth interface and full contact reaches approximately 24.5%, highlighting the significant influence of the soil–rock interface condition. To evaluate the influence of soil–rock interaction on the stability of SRM slopes, a total

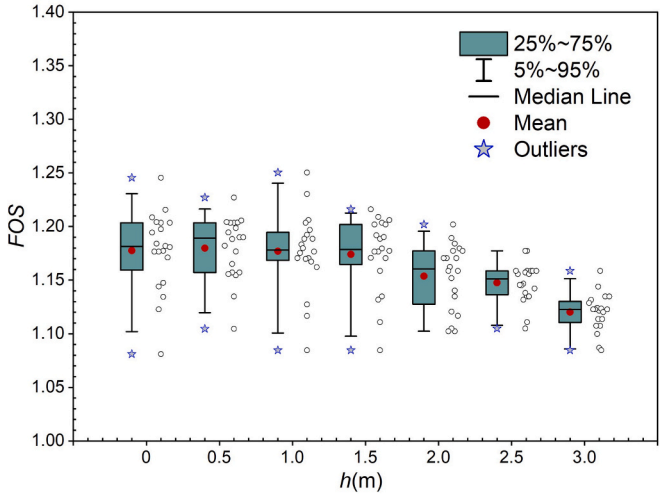

Fig. 15. Box plot of *FOS* values for SRM slopes with seven different topsoil depths (h = 0.1, 0.5, 1.0, 1.5, 2.0, 2.5, and 3.0 m) and a constant rock block content of 20%.

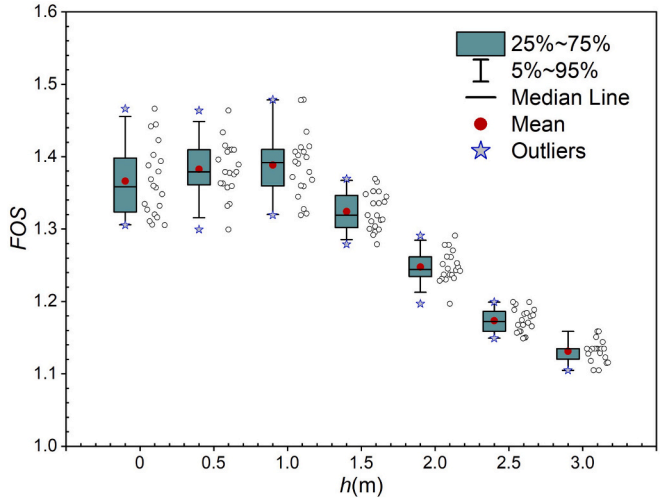

Fig. 16. Box plot of *FOS* values for SRM slopes with seven different topsoil depths (h = 0.1, 0.5, 1.0, 1.5, 2.0, 2.5, and 3.0 m) and a constant rock block content of 40%.

of 20 numerical models were developed for each topsoil thickness (0.1, 1.0, 2.0, and 3.0 m), considering rock block contents of 20% and 30% in the SRM layer. The soil–rock interaction was modeled using a frictional contact condition, with the friction coefficient defined as 0.75tanϕ'. The stability analysis results and the corresponding statistical characteristics of the *FOS* are summarized in Table 6. Comparative plots between the frictional contact cases and the full contact cases (as presented in Sections 4.1 and 4.2) are shown in Fig. 19.

As shown in Fig. 19, a reduction in soil–rock contact strength leads to a decrease in slope stability. This influence becomes less pronounced as the topsoil thickness increases and eventually becomes negligible when the topsoil layer is sufficiently thick (3.0 m). This behavior can be attributed to the reduction in soil–rock interface strength: instead of plastic deformation developing predominantly within the soil mass, relative sliding may occur along the soil–rock interface, thereby resulting in a lower factor of safety. Moreover, as the topsoil thickness increases, the proportion of rock blocks located within the potential sliding zone decreases. Consequently, the influence of soil–rock interface strength on slope stability is reduced. When the topsoil layer becomes sufficiently thick, most rock blocks in the SRM layer are located

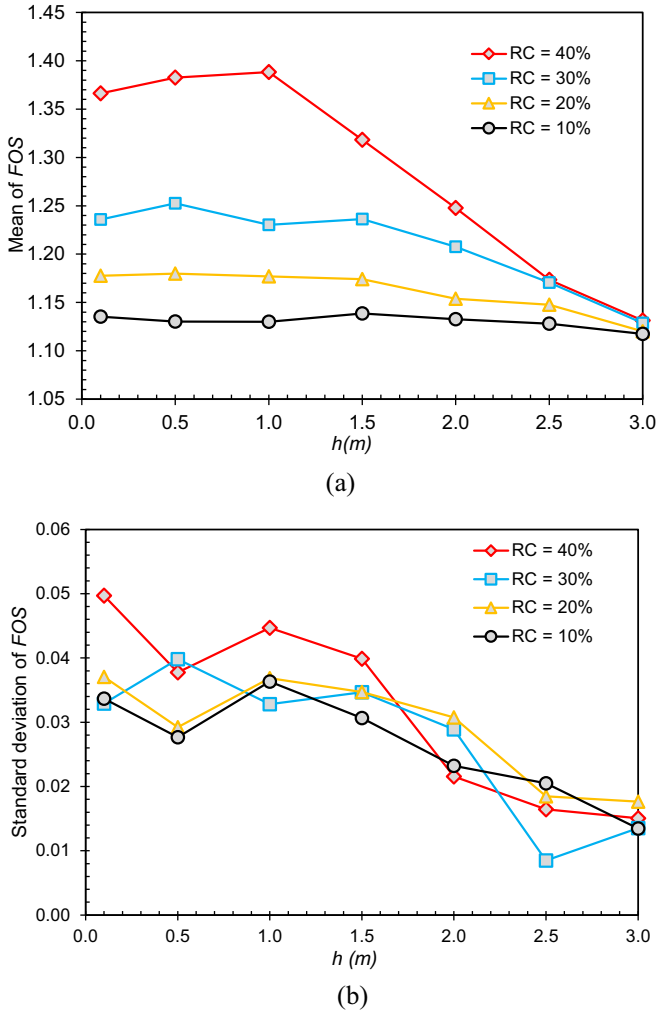

Fig. 17. Effect of rock block content (RC) in the SRM layer on the statistical characteristics of FOS: (a) Mean *FOS*, (b) Standard deviation of *FOS*.

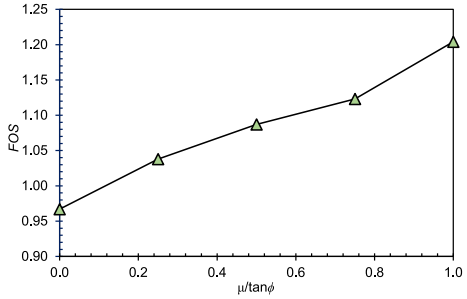

Fig. 18. Sensitivity of *FOS* to soil–rock interface friction coefficient.

outside the sliding zone, and the effect of weak soil–rock contact becomes nearly negligible. This mechanism also explains why the reduction in stability associated with decreasing interface strength is more pronounced for slopes with a higher rock block content (30%) compared with those with a lower content (20%).

5. Conclusions

In this study, SRM slope models were developed by considering the depth of the topsoil layer and varying rock block contents within the SRM layer to evaluate their combined effects on slope stability. Stability analysis was performed using the ABAQUS finite element software, applying the adaptive automatic stabilization scheme and an energy-based criterion for slope failure to determine the *FOS*. A series of numerical analyses was then conducted to investigate the influence of topsoil depth on SRM slope stability under different rock block contents and soil-rock interface strengths. The main findings are as follows:

(1) The topsoil depth significantly affects the stability of the SRM slope; however, the degree of influence depends on the rock block

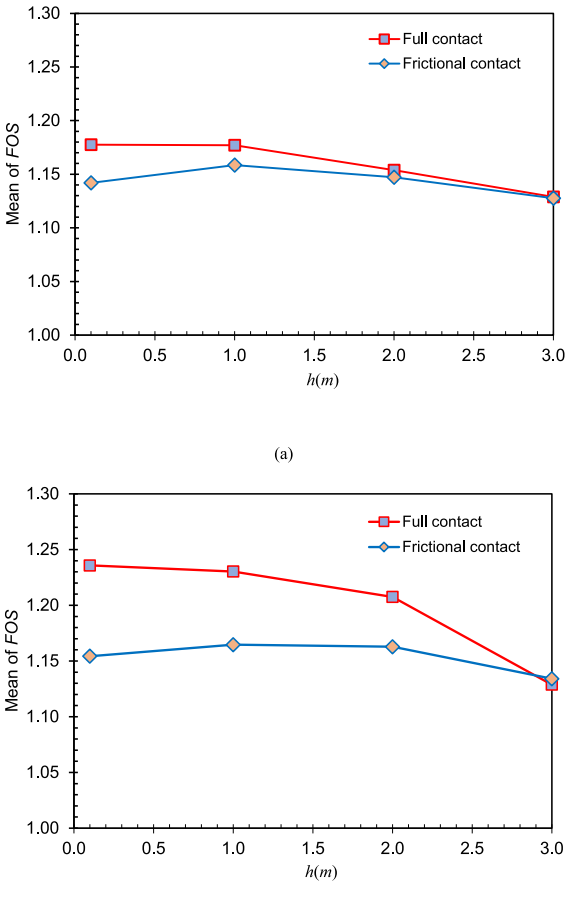

Fig. 19. *FOS* of the slope under full and frictional contact for different rock block contents: (a) 20%, (b) 30%.

Table 6
Statistical measures of *FOS* values obtained for different topsoil layer depths (h = 0.1, 1.0, 2.0 and 3.0 m) for different rock block contents of 20% and 30%.

	h (m) (rock block content of 20%)				h (m) (rock block content of 30%)			
	0.1	1.0	2.0	3.0	0.1	1.0	1.0	3.0
Mean	1.142	1.159	1.147	1.128	1.154	1.165	1.163	1.134
Max	1.177	1.177	1.186	1.137	1.186	1.197	1.187	1.177
Min	1.109	1.105	1.123	1.122	1.087	1.123	1.123	1.123
SD	0.024	0.027	0.021	0.005	0.033	0.024	0.022	0.017

content in the SRM layer. When the rock block content is low, the slope stability is less sensitive to changes in topsoil depths. Conversely, as the rock block content increases, the slope stability becomes more sensitive to topsoil depths, a reduction in stability even for shallow topsoil layers.

(2) As topsoil depth increases, slope stability tends to decrease. And, when the topsoil depth reaches 3.0 m, the differences in *FOS* values among different rock block components become negligible, indicating that the influence of the SRM layer was largely eliminated when the topsoil was sufficiently thick. Furthermore, the potential slip surface is mainly located in the topsoil layer, similar to the slip surface of a homogeneous slope.

(3) In addition, the influence of soil–rock interface strength on SRM slope stability is pronounced when the topsoil depth is shallow. The weakened interfaces promote sliding along soil–rock contacts and reduce the *FOS*. This effect decreases with increasing topsoil depth and becomes negligible when the topsoil is sufficiently thick, while slopes with higher rock block contents exhibit greater sensitivity to interface strength reduction.

The limitations of this study include the adoption of a two-dimensional plane strain assumption and simplified representations of rock block geometry and topsoil mechanical properties. In reality, slope behavior is inherently three-dimensional, and factors such as lateral confinement, sidewall friction, and complex slope geometry may significantly influence the failure mechanism and the calculated factor of safety. In addition, the investigated range of topsoil thickness is limited, and the results have not yet been validated against field observations or benchmark cases, which may constrain their direct engineering applicability. Nevertheless, the findings provide fundamental insights into the stability behavior of SRM slopes and serve as a basis for future studies incorporating three-dimensional modeling, more realistic material representations.

CRediT authorship contribution statement

Van-Hoa Cao: Writing – original draft, Validation, Software, Methodology, Investigation, Formal analysis, Data curation. **Gyu-Hyun Go:** Writing – review & editing, Visualization, Supervision, Project administration, Funding acquisition, Conceptualization. **Sinhang Kang:** Writing – review & editing, Visualization, Conceptualization.

Funding

This work was supported by the National Research Foundation of Korea(NRF) grant funded by the Korea government(MSIT) (2022R1C1C1006507, RS-2025-03192968).

Declaration of competing interest

The authors declare that they have no known competing financial interests or personal relationships that could have appeared to influence the work reported in this paper.

Data availability

Data will be made available on request.

References

Abaqus, 2018. Abaqus Analysis User's Manual 6.14–2. Dassault Systèmes Simulia Corp, Providence, RI, USA.

Abramson, L. W., Lee, T. S., Sharma, S., and Boyce, G. M., 2002. Slope Stability Concepts. Slope Stabilisation and Stabilisation Methods, Second edition, published by John Willey & Sons, Inc, pp. 329–461.

Alok, A., Burman, A., Samui, P., Kaloop, R., Eldessouki, M., 2024. A generalized limit equilibrium-based platform incorporating simplified Bishop, Janbu and Morgenstern–price methods for soil slope stability problems. Adv. Civ. Eng. 2024 (1), 3053923. https://doi.org/10.1155/2024/3053923.

Augarde, C.E., Lee, S.J., Loukidis, D., 2021. Numerical modelling of large deformation problems in geotechnical engineering: a state-of-the-art review. Soils Found. 61 (6), 1718–1735. https://doi.org/10.1016/j.sandf.2021.08.007.

Boulbes, R.J., 2020. Troubleshooting Finite-Element Modeling with Abaqus. Fransa, 1, p. 439. https://doi.org/10.1007/978-3-030-26740-7.

Brand, E.W., 1985. Predicting the performance of residual soil slopes. In: Proceedings 11th Int. Conf. Soil Mech. & Found. Engineering. San Francisco, Vol. 5, pp. 2541–2578.

Cai, H., Wei, R., Xiao, J.Z., Wang, Z.W., Yan, J., Wu, S.F., Sun, L.M., 2020. Direct shear test on coarse gap-graded fill: plate opening size and its effect on measured shear strength. Adv. Civ. Eng. 2020 (1), 5750438. https://doi.org/10.1155/2020/5750438.

Cao, V.H., Go, G.H., 2024. A novel approach to stability analysis of random soil-rock mixture slopes using finite element method in ABAQUS. Nat. Hazards 120 (15), 14381–14407. https://doi.org/10.1007/s11069–024–06771-2.

Cao, V.H., Go, G.H., 2025. Stability analysis of random soil–rock mixture slope using an energy-based failure criterion and Monte Carlo simulation. Eng. Fail. Anal., 109346 https://doi.org/10.1016/j.engfailanal.2025.109346.

Cheng, C., An, J., Kang, J., Zeng, J., Liu, F., 2023. A novel method for generation of random aggregate structure and its application in soil-rock mixture. Eng. Anal. Bound. Elem. 155, 956–965. https://doi.org/10.1016/j.enganabound.2023.07.029.

Dekking, F.M., 2005. A Modern Introduction to Probability and Statistics. Springer. pp. 234–238. (ISBN 1-85233-896-2).

Dawson, E.M., Roth, W.H., Drescher, A., 1999. Slope stability analysis by strength reduction. Geotech. 49 (6), 835–840.

Dyson, A.P, Tolooiyan, A., 2018. Optimisation of strength reduction finite element method codes for slope stability analysis. Innov. Infrastruct. Solut. 3 (1), 38. https://doi.org/10.1007/s41062-018-0148-1.

Dyson, A.P, Tolooiyan, A., 2019. Prediction and classification for finite element slope stability analysis by random field comparison. Comput. Geotech. 109, 117–129, 026. doi:10.1016/j.compgeo.2019.01.

Gao, W., Chen, X., Wang, X., Hu, C., 2021. Novel strength reduction numerical method to analyse the stability of a fractured rock slope from mesoscale failure. Eng. Comput. 37 (4), 2971–2987. https://doi.org/10.1007/s00366-020-00984-2.

Gao, W., Yang, H., Hu, R., 2022. Soil–rock mixture slope stability analysis by microtremor survey and discrete element method. Bull. Eng. Geol. Environ. 81 (3), 121. https://doi.org/10.1007/s10064-022-02622-1.

Gong, Y., Yao, A., Li, Y., Li, Y., Tian, T., 2022. Classification and distribution of large-scale high-position landslides in southeastern edge of the Qinghai–Tibet Plateau, China. Environ. Earth Sci. 81 (11), 311. https://doi.org/10.1007/s12665-022-10433-6.

Griffiths, D.V., Lane, P.A., 1999. Slope stability analysis by finite elements. Geotechnique 49 (3), 387–403.

He, J., Su, L., Cheng, P., Ren, S., Liu, Y., 2024. Numerical investigation of soil–rock mixture landslide runout by random field and finite elements. ASCE-ASME J. Risk Uncertain. Eng. Syst. Part A Civil Eng. 10 (2), 04024012. https://doi.org/10.1061/AJRUA6.RUENG-1177.

Hu, Y., Lu, Y., 2023. Study on soil-rock slope instability at mesoscopic scale using discrete element method. Comput. Geotech. 157, 105268. https://doi.org/10.1016/j.compgeo.2023.105268.

Hua, C., Yao, L., Song, C., Ni, Q., Chen, D., 2022. A new criterion for defining inhomogeneous slope failure using the strength reduction method. Comput. Model. Eng. Sci. 132 (2). https://doi.org/10.32604/cmes.2022.020260.

Huang, L., Huang, S., Lai, Z., 2020. On an energy-based criterion for defining slope failure considering spatially varying soil properties. Eng. Geol. 264, 105323. https://doi.org/10.1016/j.enggeo.2019.105323.

Huang, X.W., Yao, Z.S., Wang, W., Zhou, A.Z., Jiang, P., 2021. Stability analysis of soil-rock slope (SRS) with an improved stochastic method and physical models. Environ. Earth Sci. 80 (18), 649. https://doi.org/10.1007/s12665-021-09939-2.

Khorasani, E., Amini, M., Hossaini, M.F., Medley, E., 2019. Statistical analysis of bimslope stability using physical and numerical models. Eng. Geol. 254, 13–24. https://doi.org/10.1016/j.enggeo.2019.03.023.

Li, C., Chen, G., Guo, L., Gao, J., Peng, X., Yu, P., 2022. Slope stability and post-failure analysis of soil-rock-mixture using the modified 2D DDA-SPH method. Int. J. Rock Mech. Min. Sci. 157, 105170. https://doi.org/10.1016/j.ijrmms.2022.105170.

Li, J., Wang, B., Pan, P., Chen, H., Wang, D., Chen, P., 2024. Failure analysis of soil-rock mixture slopes using coupled MPM-DEM method. Comput. Geotech. 169, 106226. https://doi.org/10.1016/j. compgeo.2024.106226.

Liu, S., Huang, X., Zhou, A., Hu, J., Wang, W., 2018. Soil-rock slope stability analysis by considering the nonuniformity of rocks. Math. Probl. Eng. 2018 (1), 3121604. https://doi.org/10.1155/2018/3121604.

Liu, S., Wang, H., Xu, W., Cheng, Z., Xiang, Z., Xie, W.C., 2020. Numerical investigation of the influence of rock characteristics on the soil-rock mixture (SRM) slopes stability. KSCE J. Civ. Eng. 24 (11), 3247–3256. https://doi.org/10.1007/s12205-020-0034-1.

Lu, Y.E., Tan, Y., Li, X., 2018. Stability analyses on slopes of clay-rock mixtures using discrete element method. Eng. Geol. 244, 116–124. https://doi.org/10.1016/j.enggeo.2018.07.021.

Medley, E.W., Sanz, P.R., 2004. Characterization of bimrocks (rock/soil mixtures) with application to slope stability problems. In: Proceedings of Eurock 2004 and Geomechanics Colloquium, 53rd. Salzburg, Austria, October.

Meng, Q.X., Wang, H.L., Xu, W.Y., Cai, M., 2018. A numerical homogenization study of the elastic property of a soil-rock mixture using random mesostructure generation. Comput. Geotech. 98, 48–57. https://doi.org/10.1016/j.compgeo.2018.01.015.

Napoli, M.L., Barbero, M., Ravera, E., Scavia, C., 2018. A stochastic approach to slope stability analysis in bimrocks. Int. J. Rock Mech. Min. Sci. 101, 41–49. https://doi.org/10.1016/j.ijrmms.2017.11.009.

Napoli, M.L., Barbero, M., Scavia, C., 2021. Effects of block shape and inclination on the stability of melange bimrocks. Bull. Eng. Geol. Environ. 80, 7457–7466. https://doi.org/10.1007/s10064–21–02419-8.

Peng, X., Liu, J., Cheng, X., Yu, P., Zhang, Y., Chen, G., 2022. Dynamic modelling of soil-rock-mixture slopes using the coupled DDA-SPH method. Eng. Geol. 307, 106772. https://doi.org/10.1016/j.enggeo.2022.106772.

Riedmüller, G., Brosch, F.J., Klima, K., Medley, E.W., 2001. Engineering geological characterization of brittle faults and classification of fault rocks. Felsbau 19 (4), 13–19.

Sun, S., Xu, P., Wang, J., Wang, J., Feng, W., Li, J., Kanungo, D.P., 2014. Strength parameter identification and application of soil–rock mixture for steep-walled talus slopes in southwestern China. Bull. Eng. Geol. Environ. 73 (1), 123–140. https://doi.org/10.1007/s10064-013-0524-1.

Sun, G., Lin, S., Zheng, H., Tan, Y., Sui, T., 2020. The virtual element method strength reduction technique for the stability analysis of stony soil slopes. Comput. Geotech. 119, 103349. https://doi.org/10.1016/j.compgeo.2019.103349.

Tu, Y.L., Liu, X.R., Zhong, Z.L., Li, Y.Y., 2016. New criteria for defining slope failure using the strength reduction method. Eng. Geol. 212 (3), 63–71. https://doi.org/10.1016/j.enggeo.2016.08.002.

Wang, Z.M., Kwan, A.K.H., Chan, H.C., 1999. Mesoscopic study of concrete I: generation of random aggregate structure and finite element mesh. Comput. Struct. 70 (5), 533–544. https://doi.org/10.1016/S0045-7949(98) 00177-1.

Wang, S.N., Shi, C., Xu, W.Y., Wang, H.L., Zhu, Q.Z., 2014. Numerical direct shear tests for outwash deposits with random structure and composition. Granul. Matter 16, 771–783. https://doi.org/10.1007/s10035-014-0504-6.

Wang, S., Wu, W., Cui, D., 2022. On mechanical behaviour of clastic soils: numerical simulations and constitutive modelling. Géotechnique 72 (8), 706–721. https://doi.org/10.1680/jgeot.20.P.184.

Wang, Y., Zhang, Z., Kang, X., Xie, H., Wang, C., Liu, K., 2024. Stability analysis of soil and rock mixed slope based on random heterogeneous structure. Adv. Civ. Eng. 2024 (1), 1448371. https://doi.org/10.1155/2024/1448371.

Wibawa, Y.S., Sugiarti, K., Soebowo, E., 2018. Characteristics and engineering properties of residual soil of volcanic deposits. In: IOP Conference Series: Earth and Environmental Science, Vol. 118. IOP Publishing, p. 012041. https://doi.org/10.1088/1755-1315/118/1/012041.

Xu, W.J., 2008. Study on Meso-Structural Mechanics (M-SM) Characteristics and Stability of Slope of Soil-Rock Mixtures (S-RM). PhD diss. Institute of Geology and Geophysics, Chinese Academy of Science, Beijing.

Xu, X., Dai, Z.-H., 2017. Numerical implementation of a modified Mohr–Coulomb model and its application in slope stability analysis. J. Mod. Transp. 25, 40–51. https://doi.org/10.1007/s40534-017-0123-0.

Xu, W. J., and Hu, R. L., 2009. Conception, classification and significations of soil–rock mixture. Hydrogeol. Eng. Geol. 4(6), 50–56 (in Chinese).

Xu, W. J., Hu, L. M., Gao, W., 2016. Random generation of the meso-structure of a soil-rock mixture and its application in the study of the mechanical behavior in a landslide dam. Int. J. Rock Mech. Min. Sci. 86, 166–178. Doi: 10.1016/j.ijrmms.2016.04.007.

Yang, Y., Sun, G., Zheng, H., Qi, Y., 2019. Investigation of the sequential excavation of a soil-rock-mixture slope using the numerical manifold method. Eng. Geol. 256, 93–109. https://doi.org/10.1016/j.enggeo.2019.05.005.

Yang, Y., Chen, T., Wu, W., Zheng, H., 2021a. Modelling the stability of a soil-rock-mixture slope based on the digital image technology and strength reduction numerical manifold method. Eng. Anal. Bound. Elem. 126, 45–54. https://doi.org/10.1016/j.enganabound.2021.02.008.

Yang, Z., Du, Y., Chen, J., 2021b. Stability analysis of rock-soil mixture slope. In: IOP Conference Series: Earth and Environmental Science, Vol. 638. IOP Publishing, p. 012099. https://doi.org/10.1088/1755-1315/638/1/012099.

Yang, Z.P., Li, S.Q., Tian, X., Hu, Y.X., Li, W.K., 2022. Cumulative damage effect on debris slopes under frequent microseisms. J. Mt. Sci. 19 (3), 781–797. https://doi.org/10.1007/s11629-020-6419-2.

Yu, J., Zhang, Q., Wu, C., Jia, C., 2023. Investigation on stability of soil–rock mixture slope with discrete element method. Environ. Earth Sci. 82 (19), 449. https://doi.org/10.1007/s12665-023-11107-7.

Zhang, T., Zhang, J.Z., 2022. Numerical estimate of critical failure surface of slope by ordinary state-based peridynamic plastic model. Eng. Fail. Anal. 140, 106556. https://doi.org/10.1016/j.engfailanal.2022.106556.

Zhang, L., He, D., Zhao, S., Chen, X., Li, Y., Deng, M., 2021a. A new method for constructing finite difference model of soil-rock mixture slope and its stability analysis. Int. J. Rock Mech. Min. Sci. 138, 104605. https://doi.org/10.1016/j.ijrmms.2020.104605.

Zhang, Y., Jing, H., Dai, J., 2021b. Experimental analysis on the mechanical properties of soil– rock mixed fillers with different rock contents on a high embankment. DYNA Ingen. Indus. 96 (5). https://doi.org/10.6036/10235.

Zhao, L., Qiao, N., Huang, D., Zuo, S., Zhang, Z., 2022. Numerical investigation of the failure mechanisms of soil–rock mixture slopes by material point method. Comput. Geotech. 150, 104898. https://doi.org/10.1016/j.compgeo.2022.104898.

Zhao, J., Zhao, S., Luding, S., 2023. The role of particle shape in computational modelling of granular matter. Nat. Rev. Phys. 5 (9), 505–525. https://doi.org/10.1038/s42254-023-00617-9.

Zheng, H., Liu, D.F., Li, C.G., 2005. Slope stability analysis based on elasto-plastic finite element method. Int. J. Numer. Methods Eng. 64 (14), 1871–1888. https://doi.org/10.1002/nme.1406.

Zhou, Z., Yang, H., Wang, X., Liu, B., 2017. Model development and experimental verification for permeability coefficient of soil–rock mixture. Int. J. Geomech. 17 (4), 04016106. https://doi.org/10.1061/(ASCE)GM.1943-5622.0000768.

Zienkiewicz, O.C., Humpheson, C., Lewis, R.W., 1975. Associated and non-associated visco-plasticity and plasticity in soil mechanics. Geotechnique 25 (4), 671–689. https://doi.org/10.1680/geot.1975.25.4.671.

Zou, J., Yang, F., Yuan, W., Liu, Y., Liu, A., Zhang, W., 2023. A kinetic energy-based failure criterion for defining slope stability by PFEM strength reduction. Eng. Fail. Anal. 145, 107040. https://doi.org/10.1016/j.engfailanal.2022.107040.